Supplementary Information (SI) for Journal of Materials Chemistry C.
This journal is © The Royal Society of Chemistry 2026

Supporting Information

Detailed Investigation of Quantum Confinement Effects in $MAPbI_3$ Perovskite Quantum Dots through Cyclic Voltammetry and Ultraviolet Photoelectron Spectroscopy

Suyog Sanjay Mane, and Santosh Krishna Haram*

Department of Chemistry, Savitribai Phule Pune University, Ganeshkhind Rd, Ganeshkhind, Pune, Maharashtra, India 411007

*Corresponding Author=Email: santosh.haram@unipune.ac.in

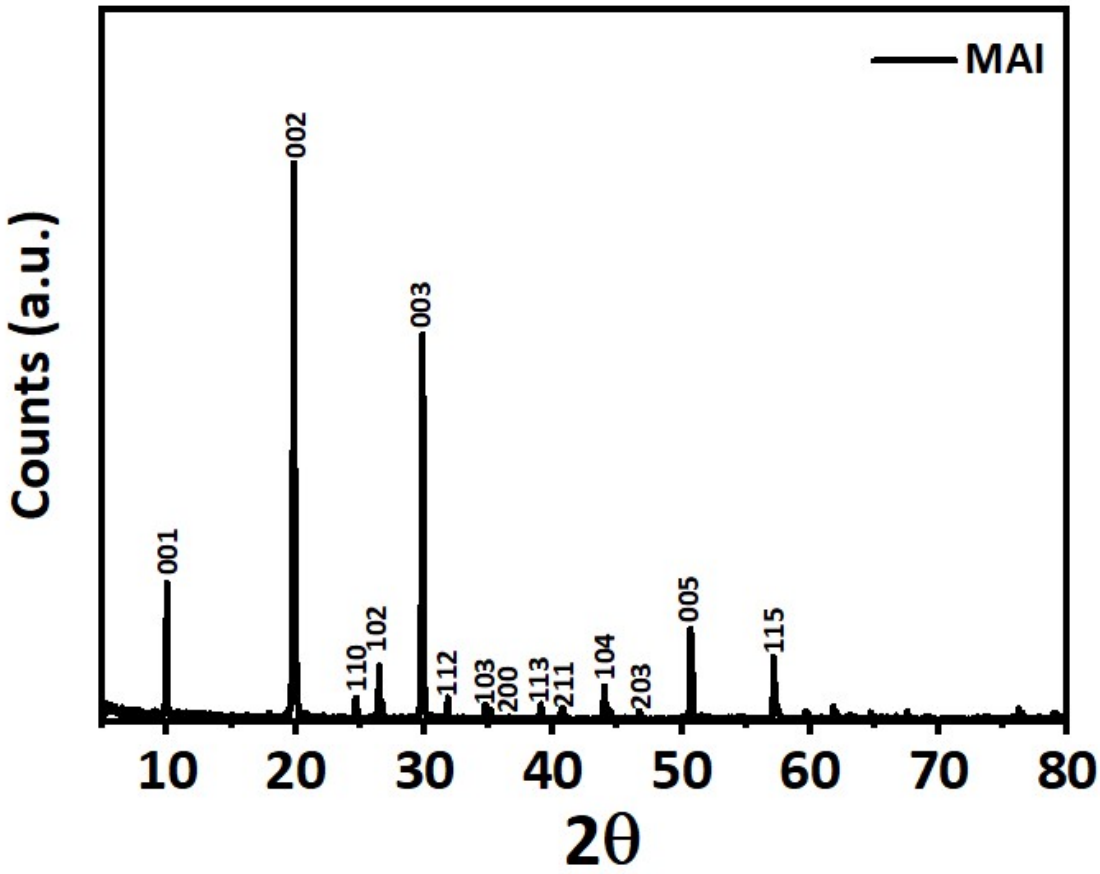

Figure S1: XRD pattern showing characteristic diffraction peaks of MAI

Figure S1 shows the powder XRD pattern of methylammonium iodide (MAI), confirming its crystalline nature and phase purity. The diffraction pattern exhibits sharp and well-resolved peaks, with the most intense reflection appearing at 2θ ≈ 19–20°, indexed to the (002) plane, which is characteristic of crystalline MAI. Additional reflections corresponding to the (001), (003), and higher-index planes further indicate long-range structural ordering within the MAI lattice.[1] The observed peak positions and their indexing are in good agreement with reported literature values for MAI, validating the formation of the desired crystalline phase. Notably, no extra diffraction peaks associated with impurity phases or unreacted species are detected, indicating high phase purity of the precursor.

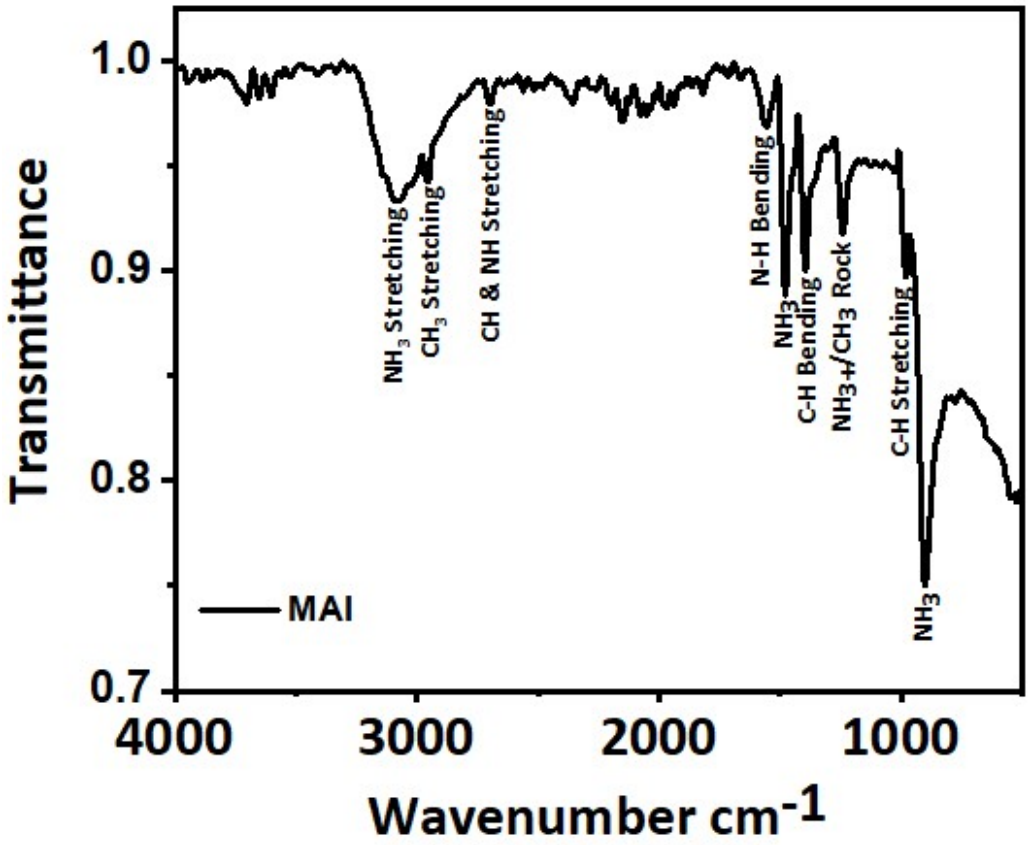

Figure S2: FTIR spectra of MAI

Figure S2 shows FTIR spectrum of methylammonium iodide (MAI) confirms the presence of characteristic vibrational modes associated with the organic methylammonium ($CH_3NH_3^+$) cation. Broad absorption bands observed in the region ~3200–3000 cm^{-1} are attributed to N–H and C–H stretching vibrations, indicating hydrogen-bonded NH_3^+ groups within the MAI lattice. The bands appearing around ~3000–2850 cm^{-1} correspond to symmetric and asymmetric C–H stretching modes of the CH_3 group. Distinct features in the region ~1650–1500 cm^{-1} are assigned to N–H bending vibrations, while peaks around ~1450–1350 cm^{-1} arise from CH_3 bending modes. The absorption bands observed in the range ~1250–1000 cm^{-1} are associated with C–N stretching and CH_3 rocking vibrations of the methylammonium ion. Additionally, a strong absorption below ~1000 cm^{-1} is attributed to NH_3^+ stretching/rocking modes, further confirming the presence of the protonated amine group. Overall, the observed FTIR bands are in good agreement with reported literature[2], validating the successful formation and chemical integrity of MAI as a perovskite precursor.

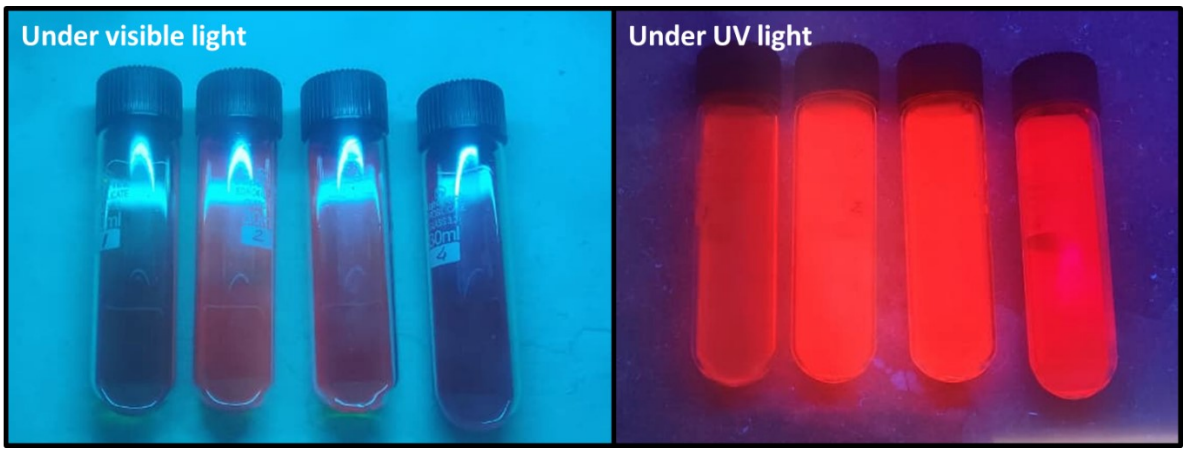

Figure S3: Digital photographs of colloidal $MAPbI_3$ PQDs dispersed in toluene under visible and UV light.

The solvent stability of $MAPbI_3$ PQDs was systematically evaluated in several commonly used electrochemical solvents, including DMF, acetonitrile, dichloromethane (DCM), propylene carbonate (PC), and DMSO, as shown in Figure S4. Figure S4(a) presents the pristine solvents prior to the addition of PQDs. After dispersing the synthesized PQDs in these solvents, noticeable differences in the appearance and stability of the dispersions were observed, as illustrated in Figure S4(b). In highly polar solvents such as DMF, acetonitrile, and DMSO, the PQDs exhibited rapid degradation or poor dispersion, which is attributed to the strong coordination ability and high polarity of these solvents that can destabilize the perovskite lattice and promote ion migration. In contrast, the dispersion in DCM appeared relatively stable with a uniform coloration, indicating better preservation of the PQD structure. Further confirmation of the solvent-dependent stability was obtained from photoluminescence observations under UV illumination (Figure S4(c)). Among the tested solvents, the PQDs dispersed in DCM displayed a strong and distinct emission, whereas the other solvents exhibited either very weak or negligible emission, suggesting significant degradation of the PQDs in those media. The strong photoluminescence observed in DCM indicates that the electronic structure and surface passivation of the PQDs remain largely intact in this solvent. A magnified image of the PQD dispersion in DCM under UV illumination is shown in Figure S4(d), clearly demonstrating its intense luminescence and stability. These observations confirm that DCM provides a more suitable environment for maintaining the structural and optical integrity of $MAPbI_3$ PQDs, making it an appropriate solvent for the electrochemical measurements performed in this study.

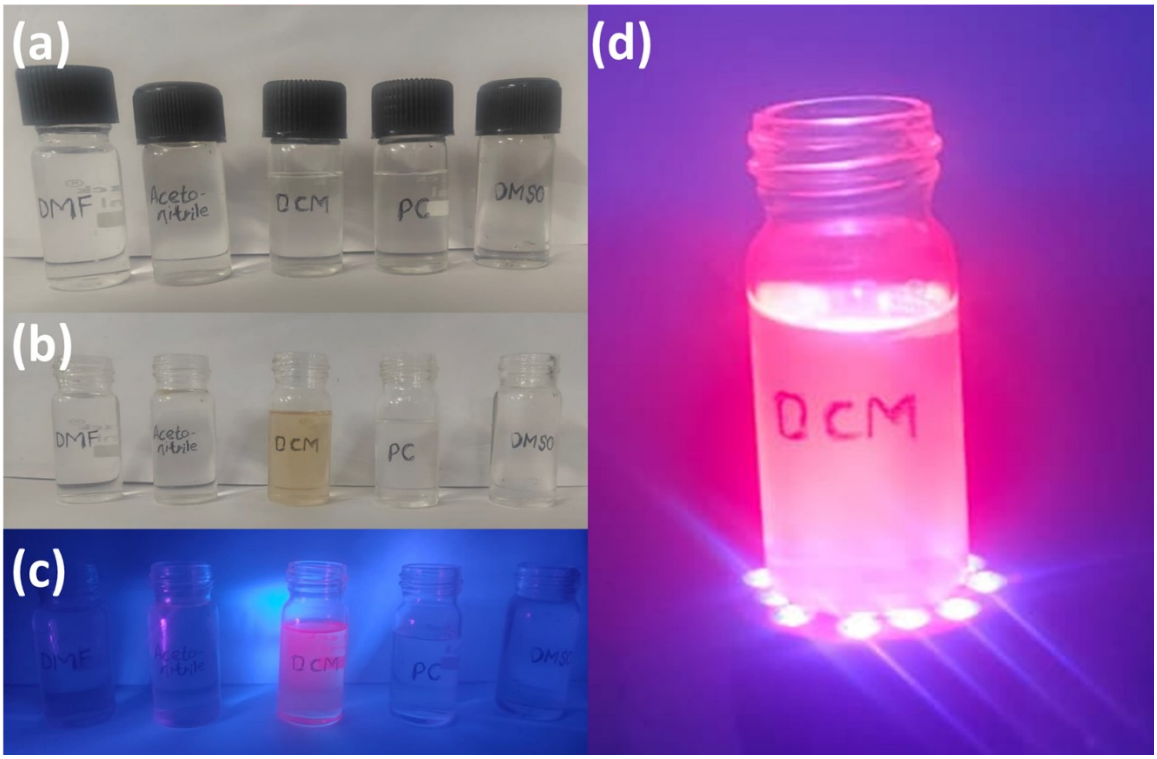

Figure S4. Photographic images demonstrating the solvent compatibility and stability of $MAPbI_3$ PQDs in different solvents. (a) Vials containing the pristine solvents: DMF, acetonitrile, DCM, propylene carbonate (PC), and DMSO. (b) Appearance of the solutions after addition of $MAPbI_3$ PQDs, showing variations in dispersion and stability across different solvents. (c) Photoluminescence response of the PQD dispersions under UV illumination, where strong emission is observed predominantly in DCM, indicating better preservation of the optical properties. (d) Enhanced photoluminescence and stability of $MAPbI_3$ PQDs dispersed in DCM, confirming it as the most suitable solvent for electrochemical measurements.

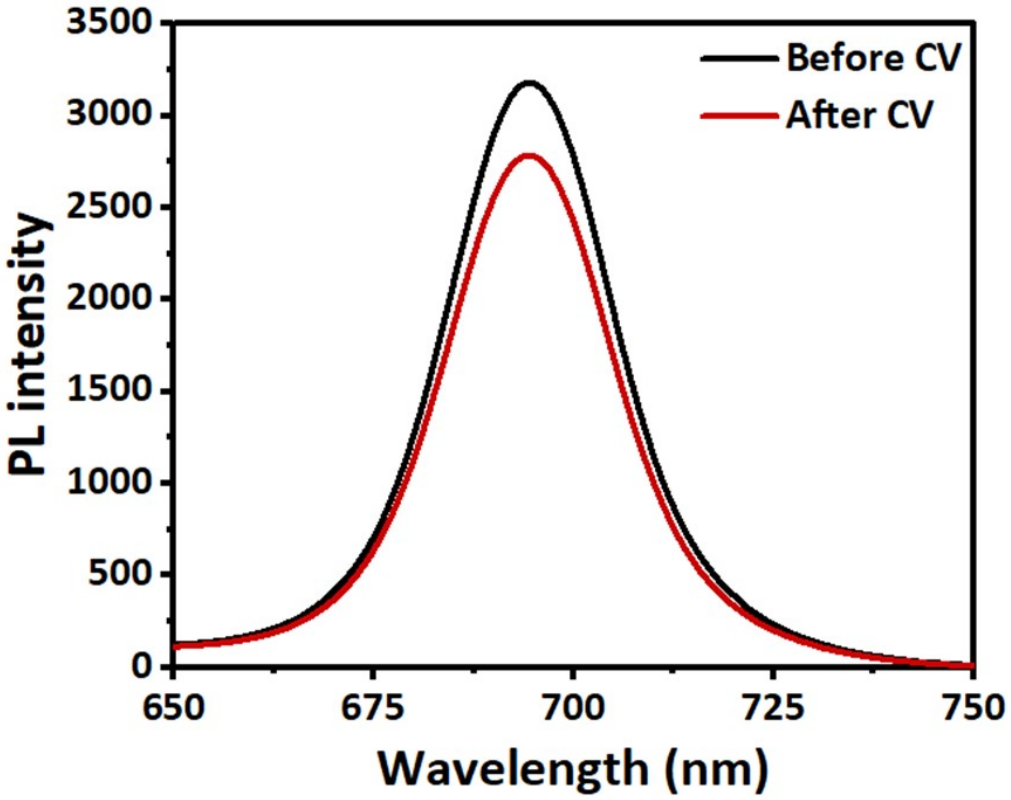

Figure S5. Photoluminescence (PL) spectra of $MAPbI_3$ PQDs recorded before and after cyclic voltammetry (CV) measurements to evaluate electrochemical stability. The negligible shift in emission peak position and only a slight decrease in PL intensity after CV indicate that the PQDs retain their structural and optical integrity, demonstrating good electrochemical stability under the applied conditions.

The Coulombic interaction energy associated with the electron–hole pair was further evaluated using the theoretical expression derived from the Brus equation (third term), which accounts for the electrostatic interaction between charge carriers in quantum-confined nanocrystals.[3] The particle radii used in the calculation were obtained from the TEM-derived particle sizes of the $MAPbI_3$ PQDs. The calculated Coulombic energy values for different particle sizes are summarized in Table S1. As expected, the Coulombic energy shows a systematic increase with decreasing particle size, which can be attributed to the reduced spatial separation between the electron and hole as well as diminished dielectric screening in smaller nanocrystals. This size-dependent trend is consistent with the enhanced quantum confinement effect observed in $MAPbI_3$ PQDs.

Table S1. Comparison of particle sizes of $MAPbI_3$ PQDs obtained from HR-TEM and Coulombic energy.

Sample	Particle size from HR-TEM (nm)	Coulombic energy (eV)	Particle size calculated from EMA (nm)
A	4.24	0.18	3.50
B	3.70	0.21	3.30
C	3.30	0.24	2.96
D	2.77	0.28	2.65
E	2.34	0.34	2.42

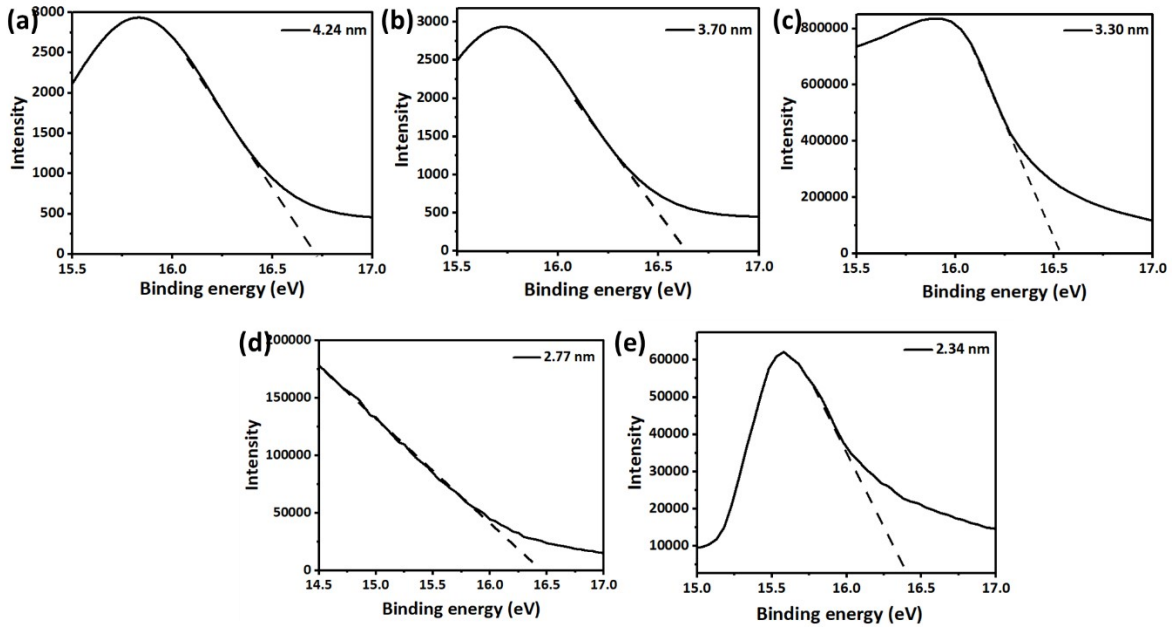

Figure S6. Ultraviolet photoelectron spectroscopy (UPS) spectra showing the secondary electron cut-off region of $MAPbI_3$ PQDs with different sizes: (a) 4.24 nm, (b) 3.70 nm, (c) 3.30 nm, (d) 2.77 nm, and (e) 2.34 nm. The dashed lines represent linear extrapolations used to determine the cut-off energy. A systematic shift in the cut-off edge with decreasing particle size indicates size-dependent variation in the work function, attributed to quantum confinement effects and surface electronic structure modifications.

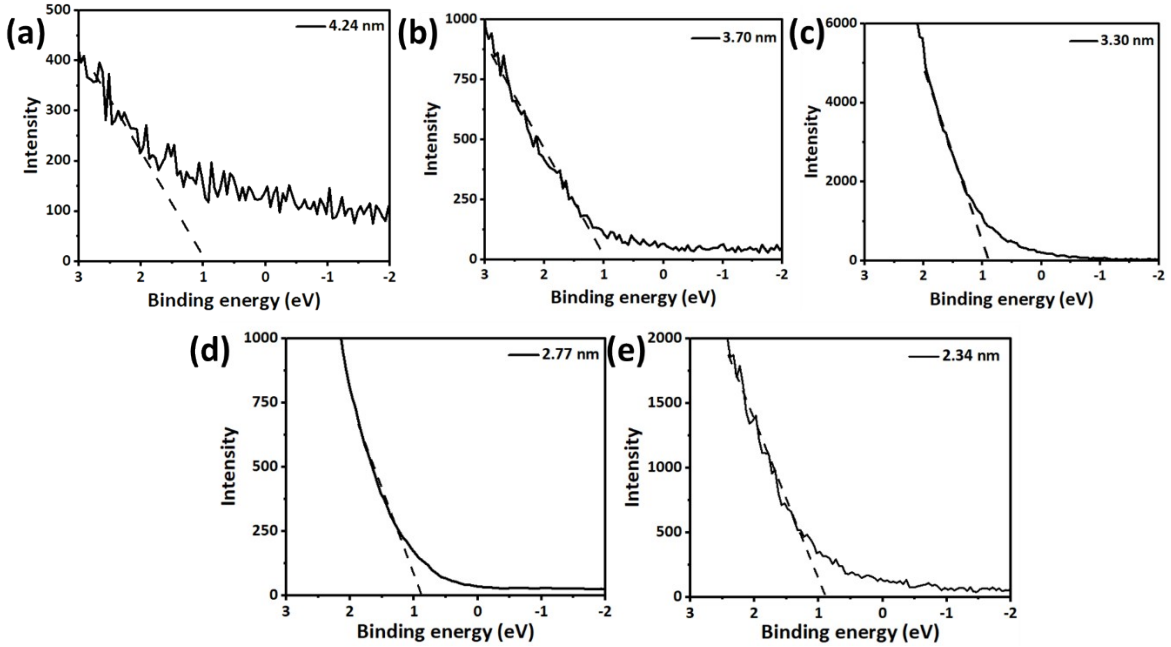

Figure S7. Ultraviolet photoelectron spectroscopy (UPS) spectra depicting the valence band maximum (VBM) region of $MAPbI_3$ PQDs with different sizes: (a) 4.24 nm, (b) 3.70 nm, (c) 3.30 nm, (d) 2.77 nm, and (e) 2.34 nm.

Table S2: Electronic parameters of $MAPbI_3$ PQDs with varying particle sizes, including cut-off energy, work function, and UPS-derived VBM and CBM levels vs. vacuum.

Particle size (nm)	**Cut off**	E_{ferni}	**Work function**	**Ultraviolet photoelectron spectroscopy**	
				VBM vs. Vacuum	CBM vs. Vacuum
4.24	16.71	0.95	4.51	-5.46	-3.85
3.70	16.64	0.93	4.58	-5.51	-3.79
3.30	16.55	0.89	4.67	-5.56	-3.78
2.77	16.47	0.85	4.75	-5.60	-3.75
2.34	16.41	0.83	4.81	-5.64	-3.72

Table S3. Size-dependent analysis of total reorganization energy (λ total) obtained from cyclic voltammetry along with the calculated Coulombic charging energy ($\mathbf{E_c}$), outer-sphere reorganization energy (λ_o) arising from solvent polarization, and the resulting inner-sphere reorganization energy (λ_i) associated with structural relaxation of $MAPbI_3$ PQDs in DCM. The values demonstrate an increase in λ_o and λ_i with decreasing particle size due to enhanced quantum confinement and stronger electron–phonon coupling in smaller PQDs.

Size (nm)	λ total (eV)	E_c (eV)	λ_o (eV)	λ_i (eV)
4.24	1.09	0.038	0.132	**0.92**
3.70	1.13	0.043	0.151	**0.94**
3.30	1.20	0.048	0.169	**0.98**
2.77	1.28	0.057	0.202	**1.02**
2.34	1.35	0.067	0.239	**1.04**

The C_1 feature is not clearly distinguishable in the original cyclic voltammograms (CV); therefore, a derivative analysis of the voltammetric curves was performed to achieve a more precise determination of the peak position. The first derivative of current with respect to potential enhances subtle variations in the signal, enabling clearer identification of peak extrema that are otherwise hidden in the raw CV data. A low-pass frequency filter was applied to the derivative curves to reduce high-frequency noise and accurately extract the true minimum corresponding to the C_1 feature. Figure S8 presents the resulting derivative profiles, which allow for a more reliable determination of the C_1 peak position. This approach ensures improved accuracy and reproducibility of the extracted peak positions across all samples.

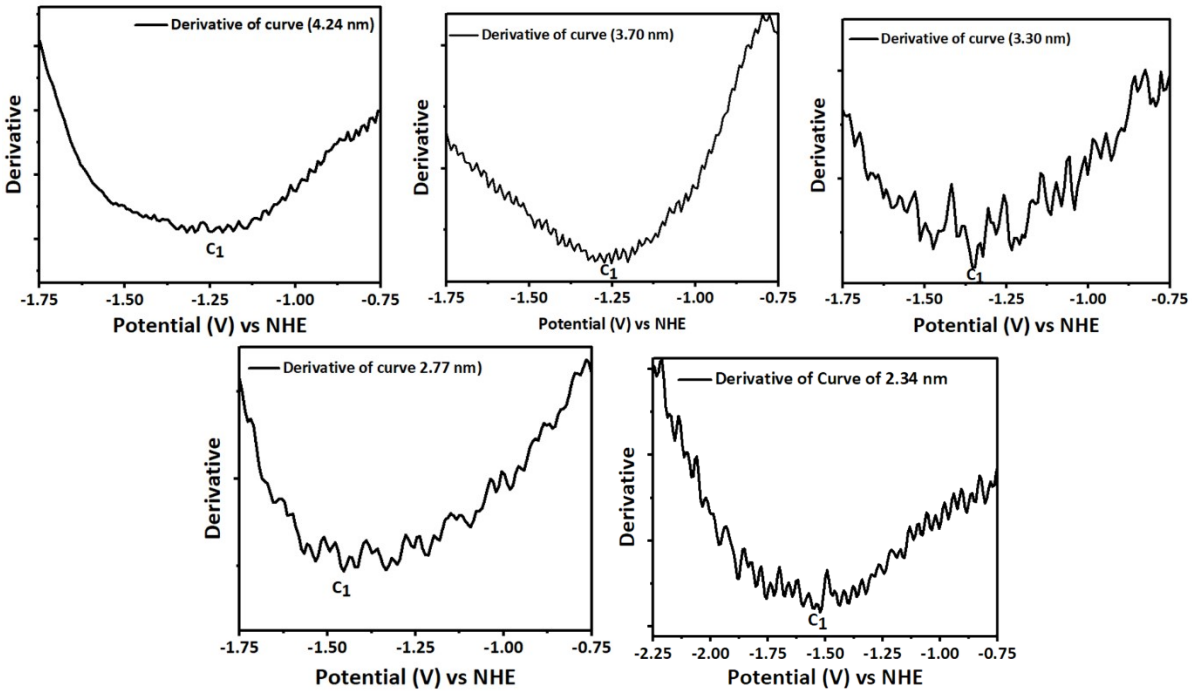

Figure S8. Derivative plots of cyclic voltammetry (CV) curves for different samples (a–e), showing the identification of the C_1 reduction feature. The derivative of current with respect to potential (dI/dV) is plotted against potential (V vs NHE) to enhance peak resolution. The minima in the derivative curves correspond to the C1 peak positions, enabling more accurate determination of peak potentials where the original CV signals were not clearly distinguishable.

Reference

(1) Gujarathi, Y. D.; Haram, S. K. Near Room Temperature Approaches for the Preparation of Air-Stable and Crystalline CH3NH3PbI3. *Mater. Chem. Phys.* **2016**, *173*, 491–497. https://doi.org/10.1016/j.matchemphys.2016.02.043.

(2) Harding, A. J.; Dobson, K. D.; Ogunnaike, B. A.; Shafarman, W. N. Thermal and Structural Characterization of Methylammonium- and Formamidinium-Halide Salts. **2021**, *2100246*, 1–6. https://doi.org/10.1002/pssa.202100246.

(3) Mane, S. S.; Uttekar J. D.; Haram S. K. Cyclic Voltammetry Investigation of Water-Stable Type II Nanoheterojunction Formation in $CsPbBr_3$– TiO_2, ChemPhysChem, e202500505, 2026, https://doi.org/10.1002/cphc.202500505